Structural analysis and magnetic properties of $(Pt/Co)_3/Pt_{tPt}/IrMn$ multilayers

L. Lechevallier,[1,*] A. Zarefy,[1] R. Lardé,[1] H. Chiron,[1] J.-M. Le Breton,[1] V. Baltz,[2] B. Rodmacq,[2] and B. Dieny[2]
[1]*Groupe de Physique des Matériaux, UMR CNRS 6634, Université de Rouen, Avenue de l'Université, BP 12, 76801 Saint Etienne du Rouvray, France*
[2]*SPINTEC (URA 2512 CNRS/CEA), INAC, CEA/Grenoble, 17 Avenue des Martyrs, 38054 Grenoble Cedex 9, France*
(Received 20 January 2009; revised manuscript received 23 March 2009; published 29 May 2009)

Structural and magnetic investigations of $Ta_{3\ nm}/[(Pt_{2\ nm}/Co_{0.4\ nm})_3/Pt_{tPt}/IrMn_{7\ nm}]_7/Pt_{10\ nm}$ multilayers with $t_{Pt}=0$ and $t_{Pt}=0.4$ nm have been carried out using x-ray reflectometry, tomographic atom probe, and superconducting quantum interference device magnetometry. The structural investigations show that the Co/IrMn interface is more diffuse in the absence of the Pt spacer. The consequences on the magnetic properties are discussed. The exchange-bias field and the anisotropy direction of these two specimens are analyzed in comparison to $Ta_{3\ nm}/[(Pt_{2\ nm}/Co_{0.4\ nm})_3/Pt_{tPt}/IrMn_{7\ nm}]/Pt_{10\ nm}$ multilayers containing only one ferromagnetic/antiferromagnetic repeat and correlated with the structural investigations.

DOI: 10.1103/PhysRevB.79.174434 PACS number(s): 75.70.Cn, 68.43.Tj

I. INTRODUCTION

When a ferromagnetic (FM) layer in contact with an antiferromagnetic (AFM) layer is field cooled from above the blocking temperature of the AFM layer, the hysteresis loop of the FM/AFM bilayer exhibits a shift, denoted as H_E for exchange-bias field, and an enhancement of the coercivity H_C due to the magnetic interactions (exchange coupling) at the FM/AFM interface.[1] This phenomenon, discovered in 1956 by Meiklejohn and Bean[2] and called exchange-bias effect, has been extensively studied during the last decades due to its applications in the development of spin electronic devices, such as spin valves and tunnel junctions.[3,4] First observed in FM/AFM bilayers exhibiting in-plane magnetic anisotropy,[1] it has been more recently evidenced in systems with out-of-plane magnetic anisotropy.[5–7] Such systems are very important for future applications because they offer the possibility of developing spin valves or tunnel junctions in high-density electronic devices with perpendicular-to-plane magnetization.[8,9] Among these different systems, ferromagnetic $(Pt/Co)_n$ (where n is the number of repeats) multilayer exchange coupled to antiferromagnetic IrMn layer can exhibit perpendicular exchange bias at room temperature.[10–17]

Recently, it has been shown that the introduction of a Pt spacer between the FM $(Pt/Co)_n$ multilayer and the AFM (FeMn or IrMn) layer strongly increases the exchange-bias field.[9–11] Considering the fact that a well-defined perpendicular magnetic anisotropy seems to be required to maximize exchange-bias field in perpendicular direction, it has been deduced that the Pt spacer leads to a reinforcement of the out-of-plane magnetic anisotropy of the FM layer.[10]

Some authors have investigated this type of samples in order to determine the mechanisms involved in the magnetization reversal. In unbiased Pt/Co/Pt trilayers[18] as in biased $(Pt/Co)_5/Pt/IrMn$,[19] they showed that the magnetization reversal is dominated by the propagation of domain walls whereas in $(Pt/Co)_5/Pt/FeMn$ (Ref. 20) the magnetization reversal is dominated by domain nucleation. For this last structure, they concluded that the mechanisms leading to the magnetization reversal strongly depend on the amplitude of the exchange-bias field.[20] In other words, the magnitude of the exchange coupling at the FM/AFM interface generating the exchange-bias field seems to influence the internal mechanism of magnetization reversal.[19]

Surprisingly, despite numerous studies on the effect of the roughness on the exchange-bias properties,[1] it seems that very few authors have directly studied the influence of the chemical intermixing at the FM/AFM interface on the exchange bias although this effect is due to the exchange coupling between the FM and AFM layers spins across this interface. Moreover, in $(Pt/Co)_n$ multilayers, the nature of interfaces plays a major role in controlling both perpendicular anisotropy and Pt magnetic polarization.[21]

In $(Pt_{2\ nm}/Co_{0.4\ nm})_n/Pt_{tPt}/IrMn_{7\ nm}$ multilayers, the reduced thickness of the layers makes the structural characterization of the interfaces extremely difficult. X-ray reflectometry, transmission electron microscopy (TEM), and nanosecondary-ion mass spectroscopy can be used to give information about thickness and roughness of the layers but information such as interface chemistry or roughness remain very qualitative in numerous cases (too many fitting parameters due to the large amount of layers, low contrast, and insufficient resolution).

It is the reason why laser-assisted tomographic atom probe (LATAP) has been used here to investigate $(Pt_{2\ nm}/Co_{0.4\ nm})_n/Pt_{tPt}/IrMn_{7\ nm}$ multilayers at the atomic scale. This technique offers an ultrahigh spatial resolution (depth resolution $\sim$0.1 nm) and provides a powerful method to observe the interface chemistry at the atomic scale.[22] Comparisons to other high-resolution analytical microscopies can be found in Ref. 23. LATAP has already been used to characterize magnetoresistive[24–26] and magnetostrictive[27] multilayers consisting of nanometric layers. We recently used LATAP to characterize the interface chemistry of FM/AFM interfaces and to evidence subnanometric layers.[28–30] The principle of the atom probe is based on ionization and evaporation of surface atoms by electric-field effect from a sample prepared in a tip shape with a top radius less than 50 nm.

In this study, using LATAP and x-ray reflectometry, we characterized the structure of sputtered $Ta_{3\ nm}/[(Pt_{2\ nm}/Co_{0.4\ nm})_3/Pt_{tPt}/IrMn_{7\ nm}]_7/Pt_{10\ nm}$ ($t_{Pt}=0$ nm and $t_{Pt}=0.4$ nm) samples, focusing the analysis on the FM/AFM

interface. In order to identify the samples, the $Ta_{3\ nm}/[(Pt_{2\ nm}/Co_{0.4\ nm})_3/Pt_{tPt}/IrMn_{7\ nm}]_7/Pt_{10\ nm}$ samples containing seven repeats of the $(Pt_{2\ nm}/Co_{0.4\ nm})_3/Pt_{tPt}/IrMn_{7\ nm}$ sequence are denoted $[ML0]_7$ and $[ML0.4]_7$ for $t_{Pt}=0$ nm and $t_{Pt}=0.4$ nm, respectively. In the same way, the $Ta_{3\ nm}/(Pt_{2\ nm}/Co_{0.4\ nm})_3/Pt_{tPt}/IrMn_{7\ nm}/Pt_{10\ nm}$ samples containing only one repeat of the $(Pt_{2\ nm}/Co_{0.4\ nm})_3/Pt_{tPt}/IrMn_{7\ nm}$ sequence are denoted ML0 and ML0.4 for $t_{Pt}=0$ nm and $t_{Pt}=0.4$ nm, respectively.

We compared the results obtained to these two measurement tools and report about the large structural difference between the Co/IrMn and Co/Pt/IrMn interfaces. We discuss the exchange-bias field values and the shape of the hysteresis loops obtained for one and seven $(Pt_{2\ nm}/Co_{0.4\ nm})_3/Pt_{tPt}/IrMn_{7\ nm}$ sequences. We finally correlate the structural and magnetic analyses by taking into account the variations of the direction of the out-of-plane magnetic anisotropy and the domain structure of the samples.

II. EXPERIMENTAL PROCEDURES

$[ML0]_7$, $[ML0.4]_7$, ML0, and ML0.4 samples were deposited at room temperature onto Si/SiO_2 plane substrates by dc magnetron sputtering using a 5.3×10^{-6} Pa base pressure and a 0.25 Pa Ar pressure during deposition. $[ML0]_7$ and $[ML0.4]_7$ samples were simultaneously deposited onto a prepatterned substrate consisting of an assembly of flat-topped Si (100) posts. The silicon posts (100 μm height and 10×10 μm^2 area) were obtained after patterning of a Si wafer by a Bosch process.[31] The samples were annealed at 550 K (above the blocking temperature of the IrMn layer) for 1 h and cooled under a field of 2.4 kOe applied perpendicular to the film plane to set the unidirectional exchange anisotropy in this direction. After deposition, the posts were picked off from the wafer, glued at the top of a thin rod with conductive epoxy glue, and tip-shaped using a focused Ga ion beam.[25] The fact that the $(Pt/Co)_3/Pt_{tPt}/IrMn$ sequence has been repeated 7 times makes specimens thick enough to allow an accurate analysis of the interfaces in regions which have remained undamaged by the Ga^{2+} ion beam during the sharpening process of the tip. Prepared tips were analyzed by LATAP at 80 K in an ultrahigh vacuum chamber at a 10^{-8} Pa pressure.

The principle of atom probe is based on the field evaporation of surface atoms as ions and their identification by time-of-flight mass spectrometry. The high electric field required (a few tens of V/nm) is obtained by applying a high voltage to the sample prepared in the form of a sharply pointed needle (tip radius less than 50 nm). The tip is biased at a high-positive dc voltage V_o in the 2–10 kV range and cooled to low temperatures (20–80 K). The vacuum in the analysis chamber is usually in the 10^{-8} Pa range. Surface atoms are then field evaporated by means of high-frequency (100 kHz) laser pulses superimposed on the dc voltage V_o.[32] The femtosecond-laser-pulsed system used is an amplified ytterbium-doped laser (amplitude system *s* pulse) with a pulse length of 350 fs. The evaporated atoms are collected by a time-resolved position detector located in front of the sample. It allows to measure the time of flight of each ion and to record its impact position. Both informations allow to deduce the chemical nature of evaporated ions and to calculate the position from which atoms originate at the tip surface. The lateral positions of atoms at the surface of the tip sample are obtained from a reverse projection of ion impact coordinates on the position sensitive detector. The depth position is deduced from the order of detection of atoms.[33] The sample is field-evaporated atomic layer per atomic layer, and a 10^4 nm^3 typical volume is collected in a few hours. After the three-dimensional (3D) reconstruction of the analyzed volume, the spatial distribution of atoms is observable at the atomic scale in the real space. From the data set of the 3D reconstruction, chemical composition or concentration depth profiles can be calculated everywhere in the analyzed volume. In the case of subnanometric layers, the use of LATAP for the determination of both thickness and composition of the layers leads in the atomic concentration profiles to a broadening of the peaks characteristic of these layers. A model that considers both the physics of field emission and the 3D reconstruction process has been developed to account for the peak broadening, thus providing an accurate structural characterization of subnanometric layers, leading to an estimation of their thickness, roughness, and chemistry of their interfaces.[30]

The $[ML0]_7$ and $[ML0.4]_7$ samples deposited on Si-plane substrates were characterized by x-ray reflectometry using a Bruker D8 system. The x-ray generator was equipped with a Co anticathode using $Co(K_{\alpha1})$ radiation ($\lambda=0.178\ 897$ nm). The corresponding reflectometry curves were fitted using SIMULREFLEC program using the classical Parat formalism including Nevot-Croce interfacial factors to account for the roughness.[34]

The magnetic properties of $[ML0]_7$, $[ML0.4]_7$, ML0, and ML0.4 samples deposited onto Si-plane substrates were investigated using a Quantum Design (MPMS XL 5T) superconducting quantum interference device (SQUID) magnetometer. Hysteresis loops were obtained with the magnetic field applied perpendicular to the film direction.

III. RESULTS

A. Structural investigation

Figure 1 shows the experimental and fitted x-ray reflectometry curves obtained for the two $[ML0]_7$ and $[ML0.4]_7$ samples. The two experimental curves show numerous peaks which characterize well-defined layers. Although the structures of these two samples are very similar, the two reflectometry curves display significant differences between 3° and 5°. The important number of layers in the samples requires using a high number of parameters to fit the reflectometry curves. Thus, we fitted the curves using different values for the thickness and roughness of all the layers and calculated the mean values of the roughness and thickness of each layer for one sequence of the two samples. Preliminary fittings made by fixing the roughness and the thickness of each layer at the same value for the seven sequences have led to similar results and revealed the same tendencies. The mean values of the thickness and roughness of the different layers are given in Table I. We note that both the roughness itself and the

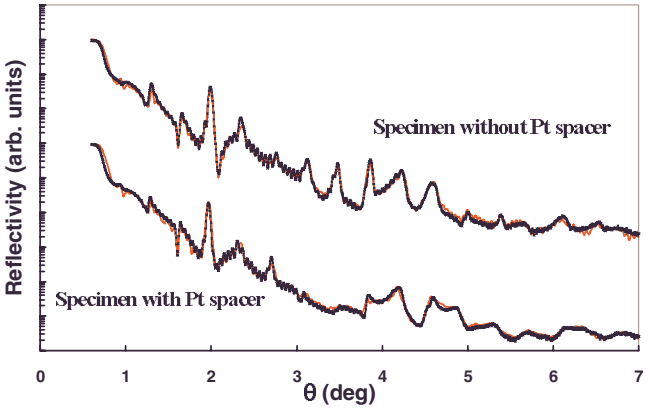

FIG. 1. (Color online) Experimental (black line) and fitted (red line) x-ray reflectometry curves obtained for the two $[ML0]_7$ and $[ML0.4]_7$ samples.

interfacial intermixing contribute to the reported roughness parameter. In order to correctly identify the layers, the first Pt layer deposited on IrMn is named $Pt_{(1)}$. It is covered during the deposition sequence by the $Co_{(1)}$, $Pt_{(2)}$, $Co_{(2)}$, $Pt_{(3)}$, and $Co_{(3)}$ layers, successively. For the two specimens, the mean thicknesses of the different layers are close to the nominal values, except for the Co_3 layer of the spacer-free specimen, which is smaller (0.23 nm) than the nominal value (0.40 nm). The roughness of the different layers is close to 0.4 nm, except also for the $Co_{(3)}$ layer, which is larger for the spacer-free sample (1.18 nm) than for the spacer-containing sample (0.90 nm). The small thickness and the high roughness of the $Co_{(3)}$ layer of the spacer-free sample with respect to the spacer-containing sample might be a consequence of the fact that the Pt spacer decreases the intermixing at the Co/IrMn interface, as this will be confirmed by our further LATAP analysis. Thus, the high number of parameters used to fit the reflectometry curves does not allow obtaining a high accuracy but only tendencies for the values of roughness and thickness of the different layers. In order to get more information on the chemical structure of the layers and the interfaces of these two samples, we have performed LATAP analysis.

TABLE I. Thickness and roughness of the different layers in $[ML0]_7$ and $[ML0.4]_7$ samples measured by x-ray reflectometry. The reported values correspond to mean values obtained for the seven sequences fitted separately.

	Thickness and roughness (nm ± 0.1)	
Layer	t_{Pt}=0 nm	t_{Pt}=0.4 nm
IrMn	6.55,0.46	6.35,0.51
Pt_x		0.45,0.44
$Co_{(3)}$	0.23,1.18	0.34,0.87
$Pt_{(3)}$	1.93,0.28	1.88,0.40
$Co_{(2)}$	0.42,0.34	0.32,0.41
$Pt_{(2)}$	1.97,0.48	2.00,0.47
$Co_{(1)}$	0.50,0.35	0.40,0.40
$Pt_{(1)}$	1.82,0.45	1.85,0.52

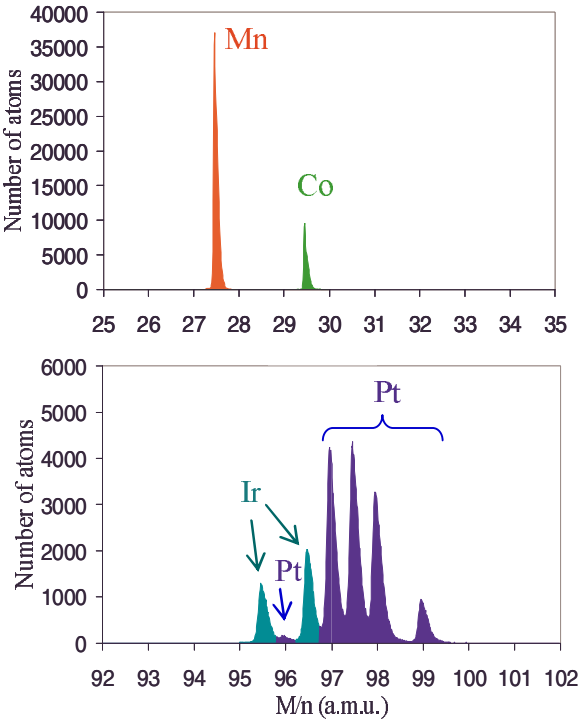

FIG. 2. (Color online) Mass spectrum of the $[ML0]_7$ sample obtained by LATAP (a) between 25 and 35 a.m.u. to characterize the Co^{2+} and Mn^{2+} peaks and (b) between 92 and 102 a.m.u. to characterize the five Pt^{2+} peaks and two Ir^{2+} peaks.

As shown in Fig. 2, the Mn, Co, Ir, and Pt atoms are the main elements detected during the LATAP analysis. All peaks of the mass spectrum corresponding to these atoms are clearly defined and well separated allowing an accurate measurement of the atomic compositions. Figure 3 shows the spatial distribution of Mn and Co atoms in approximately one $(Pt/Co)_3/Pt_{tPt}/IrMn$ sequence of the two samples. The reconstructed volumes ($5\times5\times20$ nm^3) are oriented in order to image the interfaces in cross section.

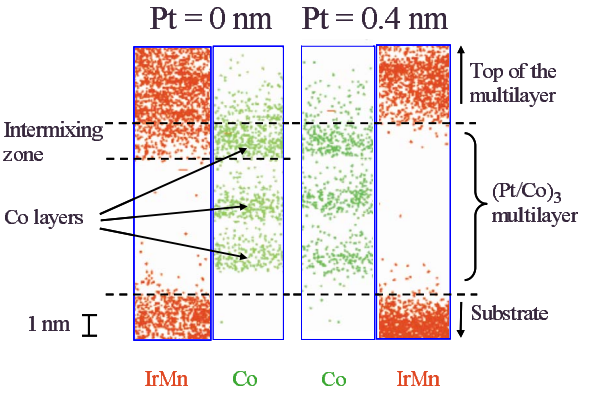

FIG. 3. (Color online) 3D reconstruction of a volume representing one sequence of the two $[ML0]_7$ and $[ML0.4]_7$ samples. Spatial distribution of Mn, Ir, and Co atoms shows a strong intermixing between IrMn and Co for the specimen without spacer (on the left) and no intermixing between IrMn and Co for the specimen with spacer (on the right).

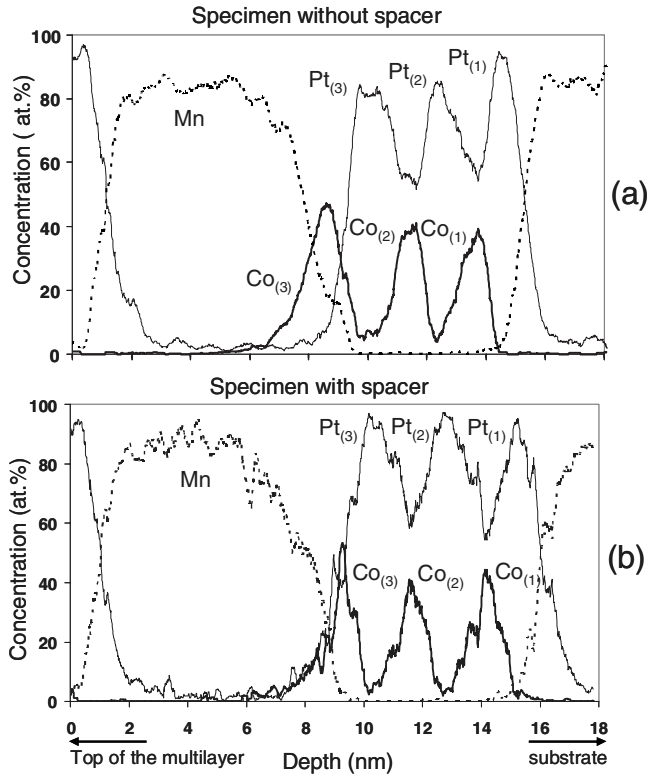

FIG. 4. Concentration profiles of the Pt, Co, and Mn atoms corresponding to the 3D reconstruction of one sequence of the two $[ML0]_7$ and $[ML0.4]_7$ samples: (a) for t_{Pt}=0 nm and (b) for t_{Pt}=0.4 nm. For the sake of clarity the Ir profile is not represented but is equivalent to the Mn one.

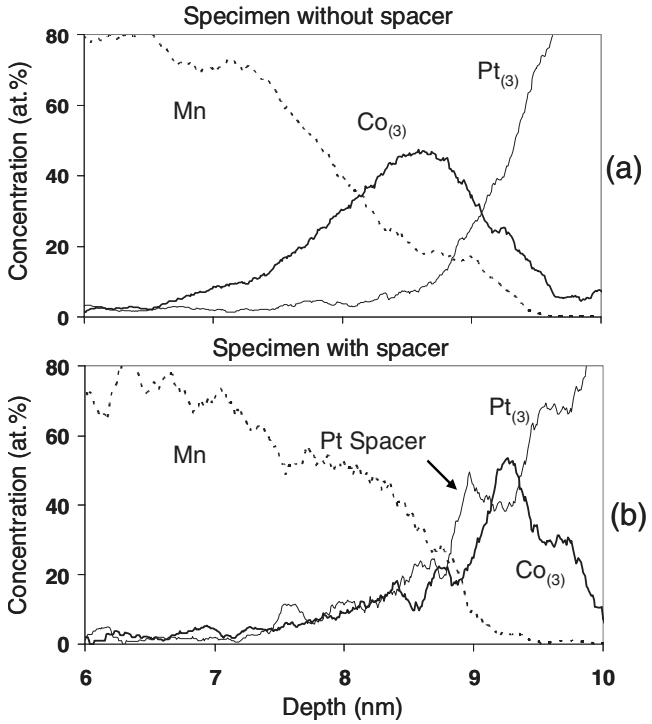

FIG. 5. Concentration profiles of Pt, Co, and Mn atoms corresponding to the 3D reconstruction of one sequence of the two $[ML0]_7$ and $[ML0.4]_7$ samples. Enlargement of Fig. 4 in the region close to the FM/AFM interface: (a) for t_{Pt}=0 nm and (b) for t_{Pt}=0.4 nm.

In the spacer-free sample, Ir and Mn atoms are present in the $(Pt/Co)_3$ multilayer on the whole thickness of the $Co_{(3)}$ layer, thus characterizing a strong intermixing between the Co atoms of the $Co_{(3)}$ layer and the Ir and Mn atoms at the Co/IrMn interface. By contrast, in the spacer-containing specimen, Ir and Mn atoms are well separated from the $Co_{(3)}$ layer leading to a sharper Co/IrMn interface. In this last case, Ir and Mn atoms do not enter the $Co_{(3)}$ layer. It results that the Co/IrMn interface is more diffuse in the absence of a Pt spacer than in the presence of a Pt spacer. In the spacer-containing sample, the Pt spacer prevents from the diffusion of the Ir and Mn atoms through the $Co_{(3)}$ layer.

The concentration profiles of the Pt, Co, and Mn atoms, corresponding roughly to one sequence of the two samples, are shown in Fig. 4. For the sake of clarity, the Ir profile that is connected to the Mn ones is not represented. Figures 5(a) and 5(b) are enlargements of Figs. 4(a) and 4(b) in the region close to the FM/AFM interface.

For the two samples, the concentration profiles of the Co and Pt atoms in the $(Pt/Co)_3$ multilayer are similar except for the $Co_{(3)}$ layer. For the spacer-free sample, a simple convolution model, which takes into account the Co peak shape and the physics of field emission applied to an atom probe, allowed to deconvolute the peaks representing the three subnanometer Co layers, leading to their structural characterization.[30] In other words, the uncertainties in position associated with the field emission being of the same order of magnitude as the nominal thickness of the Co layers (~0.4 nm) result in a slight experimental overestimate of these peaks, which requires deconvolution. The distribution of Co atoms in the three Co layers of the two samples obtained from the experimental profiles is presented in Fig. 6. Thus, for the two samples, the $Co_{(1)}$ and $Co_{(2)}$ layers (deposited on the $Pt_{(1)}$ and $Pt_{(2)}$ layers) are slightly intermixed with Pt and extend roughly over four atomic planes, with two Co-rich planes in the middle of the layer and sharp Co/Pt interfaces of one monolayer on each side. This result is in agreement with those obtained in Refs. 21, 35, and 36. In contrast, the concentration profile of the $Co_{(3)}$ layer is very different for the two samples. For the spacer-free sample (Fig. 6), the peak representing the $Co_{(3)}$ layer is broader than the $Co_{(1)}$ and $Co_{(2)}$ ones. The $Co_{(3)}$ layer roughly extends over seven atomic planes.[30] In Fig. 5(b), one can observe that the Co atoms are strongly intermixed with Mn and Pt atoms in the whole thickness of the $Co_{(3)}$ layer; the Mn concentration becoming negligible when the Pt concentration strongly increases. For the spacer-containing sample (Fig. 6), the peak representing the $Co_{(3)}$ layer has approximately the same shape and extension as the $Co_{(1)}$ and $Co_{(2)}$ ones. This indicates that the $Co_{(3)}$ layer also extends roughly over four atomic planes. This shows that the Pt spacer is as efficient against intermixing as the other Pt layers, despite its very small thickness. One can also deduce that the Pt spacer is likely a compact layer, weakly intermixed, with a thickness close to two atomic planes (0.4 nm). It results that the Co atoms of the $Co_{(3)}$ layer are very weakly intermixed with Mn and Pt.

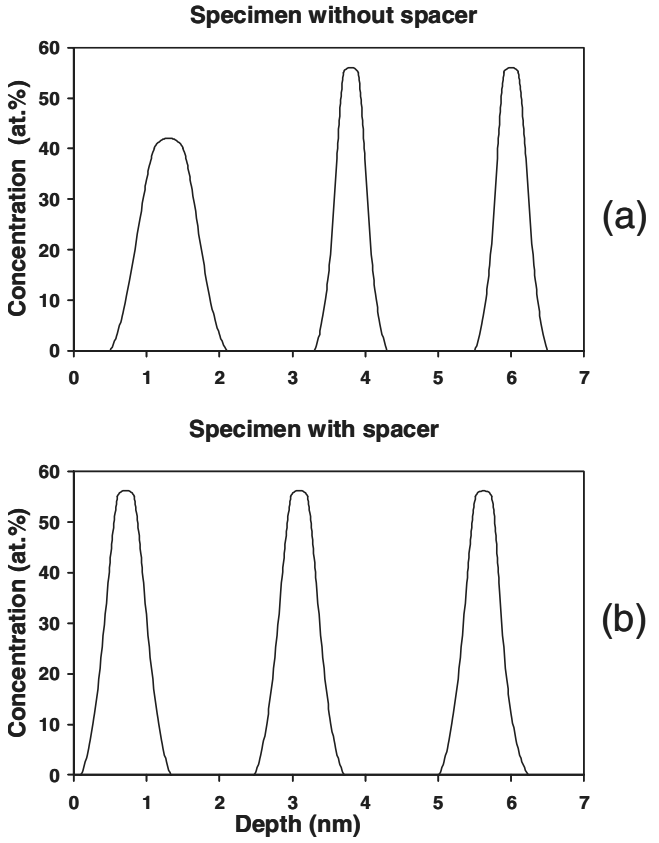

FIG. 6. Distribution of the Co atoms in the three Co layers deduced from the Co modeled concentration profiles (Ref. 30). (a) For the sample without Pt spacer and (b) for the sample with a Pt spacer.

The positions of the Pt atoms in the $(Pt/Co)_3$ multilayer are displayed in Fig. 7. The Pt atomic planes can be clearly observed in the two Pt layers deposited on Co layers (i.e., $Pt_{(2)}$ and $Pt_{(3)}$ layers). Having the $(Pt/Co)_3$ multilayer exhibiting a (111) weak texture[10] and the distance between two Pt (111) atomic planes being equal to 0.2266 nm, we can thus estimate the thickness of the crystalline zones (see Fig. 7). Between the two Pt crystalline zones, a Co layer can be identified with a thickness smaller than 1 nm.

The (111) crystalline texture does not appear in the $Pt_{(1)}$ layer in contact with IrMn. It is known that the (111) Pt texture strongly depends on the buffer layer.[10,37] One can deduce that the IrMn layer is not a satisfactory buffer for promoting a good (111) texture and that the Co layers act as better buffers than IrMn in promoting (111) Pt texture.

One can observe in Fig. 5(b) a small peak corresponding to the 0.4-nm-thick Pt spacer. It clearly appears that the Mn concentration strongly decreases when the Pt concentration increases. This is due to the presence of the Pt spacer. The Mn concentration being almost negligible in the whole thickness of the $Co_{(3)}$ layer, the Pt spacer seems to prevent the diffusion of the Mn atoms in this layer during the deposition process. The Pt spacer thus acts as a diffusion barrier for the migration of Mn toward the $Co_{(3)}$ layer. In other words, Mn (but also Ir) is thought to diffuse much slower in Pt than in Co.

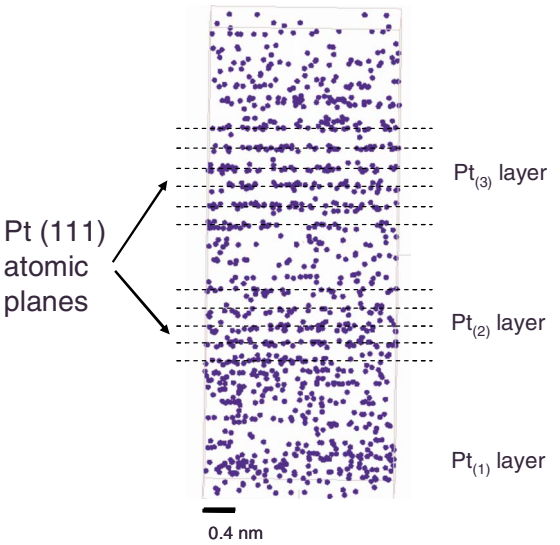

FIG. 7. (Color online) 3D reconstruction of one $(Pt/Co)_3$ multilayer of the $[ML0]_7$ sample showing the spatial distribution of Pt atoms. The Pt (111) atomic planes in the regions corresponding to the $Pt_{(2)}$ and $Pt_{(3)}$ layers deposited on Co layers are clearly evidenced.

In the spacer-free sample, a strong intermixing between Ir, Mn, and Co atoms occurs during IrMn layer deposition on the $Co_{(3)}$ layer. Ir and Mn atoms diffuse through the whole thickness of the $Co_{(3)}$ layer down to the $Pt_{(3)}$ layer where they are stopped. In the two samples, the Pt spacer and the $Pt_{(3)}$ layer (for the spacer-free sample) act as diffusion barriers.

In multilayers, both the chemical nature and roughness of the interfaces, in relation with the possible atomic intermixing, influence the magnetic properties, such as the exchange-bias effect. These parameters are closely related to the growth mechanisms involved during the deposition of the different layers. In the case of multilayers obtained by magnetron sputtering, the high-impact energy can cause interface smoothening during deposition, as observed for island-growth processes.[38,39] It can also induce atomic intermixing at the interfaces.[24] During deposition, ballistic phenomena occur which can lead to the penetration of incident atoms into the layers and to the ejection of surface atoms. This impact-induced interdiffusion mechanism increases with the impact energy and varies according to the chemical nature of the atoms.[39] This phenomenon can be characterized by an exchange probability between an impacting atom and a surface atom. A high value of the exchange probability yields a diffuse interface.[24] In the case of CoFe/Cu/CoFe trilayer, it was shown that the high values of the exchange probabilities of Fe and Co impacting Cu resulted in a diffuse Cu/CoFe interface whereas the low value of the Cu exchange probability impacting Co or Fe was associated with a sharp CoFe/Cu interface.[24] Thus, for the two samples investigated here, the exchange probability of the Ir and Mn atoms impacting the Co atoms of the $Co_{(3)}$ layer is likely higher than the exchange probability of the Ir and Mn atoms impacting the Pt atoms of the Pt spacer covering the $Co_{(3)}$ layer. The fact that the Pt atomic weight is much higher than that of Co very likely

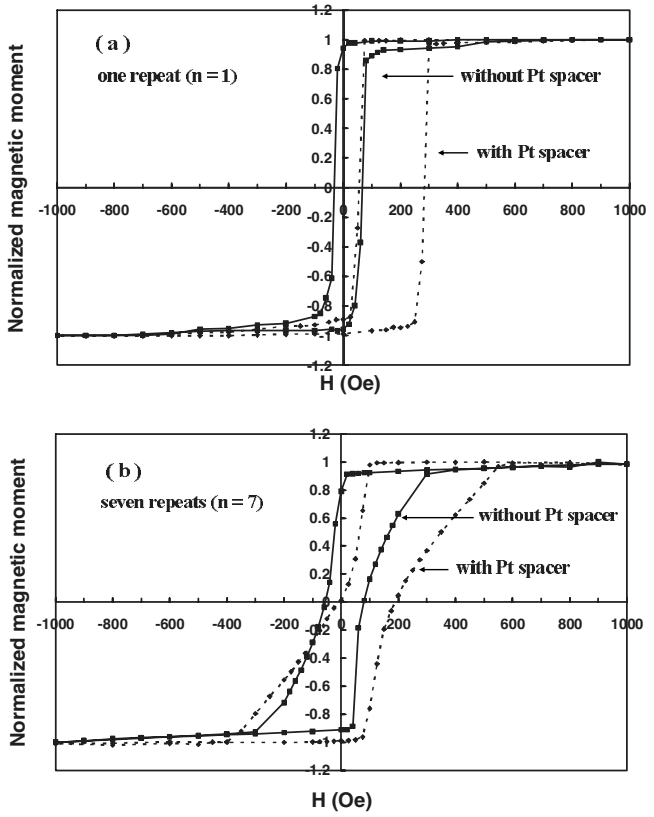

FIG. 8. Hysteresis loops of the $[ML0]_7$, $[ML0.4]_7$, ML0, and ML0.4 samples measured at room temperature by SQUID magnetometry after cooling from 550 K under a 2.4 kOe magnetic field applied in the direction perpendicular to the film plane: (a) for one repeat ($n=1$) and (b) for seven repeats ($n=7$).

limits the impact-induced interdiffusion mechanism for the sample containing a Pt spacer and thus the intermixing between the Ir, Mn, Pt, and Co atoms. In this case, the Pt spacer acts as a ballistic diffusion barrier.

It is worth mentioning that the Co melting point is lower than the Pt one. This could suggest that the Ir and Mn incident atoms would thermally exchange more easily with the Co atoms than with the Pt atoms. In this case, for the spacer-free sample, the high diffusion between the different atoms at the Co/IrMn interface would be induced by a thermal process. According to these considerations, the Pt spacer would also act as a thermal diffusion barrier.

B. Magnetic properties

The hysteresis loops of the $[ML0]_7$, $[ML0.4]_7$, ML0, and ML0.4 samples were measured at room temperature by SQUID magnetometry, the magnetic field being applied perpendicular to the film plane. The two samples containing seven repeats present bottom $Co_{0.4\ nm}/Pt_{tPt}/IrMn_{7\ nm}$ interfaces but also top $IrMn_{7\ nm}/Pt_{2\ nm}/Co_{0.4\ nm}$ ones.[40] Given the large thickness of the Pt spacer for the top interface,[10] we can consider that the exchange-bias interaction is only due to the magnetic moments located at the bottom $Co_{0.4\ nm}/Pt_{tPt}/IrMn_{7\ nm}$ interface.

The hysteresis loops of the four samples are shown in Fig. 8. From Fig. 8(a), we observe that for one repeat ($n=1$) of the $(Pt_{2\ nm}/Co_{0.4\ nm})_3/Pt_{tPt}/IrMn_{7\ nm}$ sequence, both ML0 and ML0.4 samples display square hysteresis loops, as previously ascribed to a strong out-of-plane anisotropy.[10,40] The addition of a Pt spacer between the FM $(Pt_{2\ nm}/Co_{0.4\ nm})_3$ multilayer and the AFM $IrMn_{7\ nm}$ layer results in an enhancement of the exchange bias:[10,40] here, for $t_{Pt}=0$, one measures $H_E=17$ Oe, whereas for $t_{Pt}=0.4$ nm one gets $H_E=115$ Oe. The above result has already been ascribed to some improvement of the out-of-plane orientation of the $Co_{(3)}$ layer magnetization within the multilayer due to the addition of a Co-Pt interface and thus to an additional interfacial out-of-plane anisotropy energy.[10,40] However this cannot explain the order of magnitude increase in H_E.[10] Data deduced from tomographic atom probe experiments (see above Figs. 4 and 5) indicate that the Pt spacer also proves to be an efficient diffusion barrier against the interdiffusion of Ir, Mn, and Co atoms at the FM/AFM interface, thus mostly contributing to the extra out-of-plane anisotropy of the $Co_{(3)}$ layer of the $(Pt_{2\ nm}/Co_{0.4\ nm})_3$ multilayer.

From Fig. 8(b), for seven repeats of the $(Pt_{2\ nm}/Co_{0.4\ nm})_3/Pt_{tPt}/IrMn_{7\ nm}$ sequence ($n=7$), we also observe that the Pt spacer leads to an enhancement of the exchange bias: for $t_{Pt}=0$, we measure $H_E=12$ Oe whereas for $t_{Pt}=0.4$ nm, we get $H_E=90$ Oe, for the same reasons as those discussed above. However, both specimens now show nucleation in positive field, in contrast to the case of one repeat of the sequence. Additionally, the two H_E values are smaller than the ones obtained for one repeat and both loops no more exhibit a square shape but are rather slanted. We can also observe that the Pt spacer-containing sample surprisingly shows a lower susceptibility, i.e., a more tilted hysteresis loop than the free spacer sample. Such a lower value of susceptibility is a further manifestation of the enhancement of out-of-plane anisotropy due to the addition of the spacer layer, as discussed hereafter.

It is known that magnetization reversal of a magnetic layer strongly depends on its thickness.[41,42] Gehanno *et al.*[43] showed that susceptibility decreases exponentially as the thickness of the magnetic layer is increased, as a result between the balance between magnetostatic energy and domain-wall energy. This effect can also be treated in terms of a critical film thickness above which the single-domain magnetic configuration no more prevails over the multidomain one.[41,42]

Our present samples can be viewed as seven $(Pt_{2\ nm}/Co_{0.4\ nm})_3$ multilayers separated by $Pt_{tPt}/IrMn_{7\ nm}$ bilayers. The $(Pt_{2\ nm}/Co_{0.4\ nm})_3$ multilayers are surely magnetically coupled: (i) possibly via the formation of uncompensated domains (or spins) within the $IrMn_{7\ nm}$ layer[44] or (ii) more likely via magnetostatic energy terms, which favor a multidomain configuration, as detailed in Ref. 45. For the case of $(Pt/Co)_n$-based multilayers similar to ours and separated by a thick Pt spacer (from 4 to 100 nm), it has been shown that inter-$(Pt/Co)_n$ magnetostatic coupling strongly influences the macroscopic magnetization reversal of the whole stack and favors the formation of a multidomain magnetic configuration. Due to these magnetostatic interactions, the system behaves like a monolayer with increased mag-

netic effective thickness.[45] Similarly our seven $(Pt_{2\ nm}/Co_{0.4\ nm})_3$ multilayers are magnetostatically coupled via the $Pt_{tPt}/IrMn_{7\ nm}$ bilayers which also tend to favor the formation of a multidomain magnetic configuration. The whole stack also behaves like a sample with an enhanced magnetic effective thickness. It thus results that for both $t_{Pt}=0$ nm and $t_{Pt}=0.4$ nm, the magnetic susceptibility for $n=7$ is lower than the susceptibility for $n=1$, as observed in Fig. 8.

For $n=7$ and $t_{Pt}=0.4$ nm, as discussed above, the out-of-plane orientation of the topmost $Co_{(3)}$ layers of the $(Pt_{2\ nm}/Co_{0.4\ nm})_3$ multilayers, which are repeated 7 times is improved with respect to the case of $t_{Pt}=0$ nm. It thus results that the out-of-plane magnetic stray fields which appear when the system breaks into domains are larger for $t_{Pt}=0.4$ nm than for $t_{Pt}=0$ nm. The sample containing a Pt spacer thus exhibits larger intermultilayer magnetostatic interactions, which might account for the observation of a lower susceptibility with respect to the spacer-free specimen [Fig. 8(b)]. In other words, for the spacer-containing sample, the stray fields by the seven $(Pt_{2\ nm}/Co_{0.4\ nm})_3$ multilayers lead to a stronger magnetostatic coupling which favors a multidomain configuration of the whole sample. In contrast, for the sample without a Pt spacer, due to the tilted orientations of the $Co_{(3)}$ layer spins, the stray fields by the $(Pt_{2\ nm}/Co_{0.4\ nm})_3$ multilayers are lower than for the previous sample, leading to a somewhat weaker magnetostatic coupling. The magnetic configuration of the spacer-free sample is thus closer to the magnetic configuration obtained for only one repeat. The hysteresis loop obtained for the spacer-free sample is thus squarer than the hysteresis loop of the spacer-containing sample.

The absence of Pt atomic planes in the first $Pt_{(1)}$ layers of the $(Pt_{2\ nm}/Co_{0.4\ nm})_3$ multilayers (see Fig. 7), likely due to a difficult growth of the Pt (111) texture on IrMn, could explain that the two exchange fields obtained for seven repeats are smaller than the ones obtained for only one repeat. The presence of additional magnetostatic interlayer interactions results in significant differences in the hysteresis loops of stacks with a single or seven repeats of $(Pt/Co)_3$ multilayers, either separated by a single IrMn layer or by a Pt/IrMn bilayer. In the case of seven repeats, the magnetostatic interactions between the $(Pt/Co)_3$ multilayers seem to be enhanced for a Pt/IrMn separation with respect to a single IrMn separation. This is a likely consequence of the limitation of Mn diffusion in the topmost Co layers due to the Pt insertion (resulting in a higher moment of these Co layers) and to a reinforcement of the perpendicular orientation of the magnetization of these topmost Co layers in the $(Pt/Co)_3$ multilayers.

IV. CONCLUSION

The investigation by LATAP of $Ta_{3\ nm}/[(Pt_{2\ nm}/Co_{0.4\ nm})_3/Pt_{tPt}/IrMn_{7\ nm}]_7/Pt_{10\ nm}$ samples, with $t_{Pt}=0$ nm and $t_{Pt}=0.4$ nm, prepared by dc magnetron sputtering allowed us to chemically and locally characterize the different interfaces of these two samples and to reveal a strong intermixing at the Co/IrMn interface, suggested by x-ray reflectometry measurements. The analysis of concentration profiles revealed the subnanometric Co layers of the $(Pt/Co)_3$ multilayers and allowed the characterization of their chemical structure, in particular that of the $Co_{(3)}$ layer which plays a prominent role in the exchange-bias effect. The reconstruction procedure also allowed the observation of the (111) atomic planes of the Pt layers deposited on the Co layers ($Pt_{(2)}$ and $Pt_{(3)}$ layers). The nonobservation of these planes in the $Pt_{(1)}$ layer deposited on IrMn reflects a poor quality growth of Pt on IrMn.

These results were correlated with magnetometry measurements. The analysis of the hysteresis loops of samples containing one and seven repeats of the $(Pt/Co)_3/Pt_{tPt}/IrMn$ sequence showed that samples with and without a Pt spacer exhibit a single-domain magnetic configuration for one repeat and a multidomain magnetic configuration for seven repeats. In the case of seven repeats, the differences between the hysteresis loops were interpreted by higher magnetostatic interlayer interactions for the spacer-containing sample due to a larger out-of-plane anisotropy. The correlated study of the magnetic and structural analyses allowed us to show that the addition of a thin Pt layer between the topmost $Co_{(3)}$ layer of the $(Pt/Co)_3$ multilayer limits interdiffusion at the FM/AFM interface and enhances the out-of-plane orientation of the Co spins of the $(Pt/Co)_3$ multilayers, which reinforces the exchange-bias amplitude.

ACKNOWLEDGMENTS

The authors would like to thank F. Vurpillot, E. Cadel, and A. Bostel for numerous and useful discussions.

*luc.lechevallier@univ-rouen.fr

[1] J. Nogués and I. K. Schuller, J. Magn. Magn. Mater. **192**, 203 (1999).
[2] W. H. Meiklejohn and C. P. Bean, Phys. Rev. **102**, 1413 (1956).
[3] B. Dieny, V. S. Speriosu, S. S. P. Parkin, B. A. Gurney, D. R. Wilhoit, and D. Mauri, Phys. Rev. B **43**, 1297 (1991).
[4] S. Tehrani, J. M. Slaughter, M. Deherrera, B. N. Engel, N. D. Rizzo, J. Slater, M. Durlam, R. W. Dave, J. Janesky, B. Butcher, K. Smith, and G. Grynkewich, Proc. IEEE **91**, 703 (2003).
[5] S. Maat, K. Takano, S. S. P. Parkin, and E. E. Fullerton, Phys. Rev. Lett. **87**, 087202 (2001).
[6] Z. Y. Liu and S. Adenwalla, Phys. Rev. Lett. **91**, 037207 (2003).
[7] J. Sort, B. Dieny, M. Fraune, C. Koenig, F. Lunnebach, B. Beschoten, and G. Güntherodt, Appl. Phys. Lett. **84**, 3696 (2004).
[8] C. H. Marrows, Phys. Rev. B **68**, 012405 (2003).
[9] F. Garcia, J. Sort, B. Rodmacq, S. Auffret, and B. Dieny, Appl. Phys. Lett. **83**, 3537 (2003).
[10] J. Sort, V. Baltz, F. Garcia, B. Rodmacq, and B. Dieny, Phys. Rev. B **71**, 054411 (2005).
[11] S. van Dijken, J. Moritz, and J. M. D. Coey, J. Appl. Phys. **97**,

063907 (2005).
[12] J. Sort, F. Garcia, B. Rodmacq, S. Auffret, and B. Dieny, J. Magn. Magn. Mater. **272-276**, 355 (2004).
[13] R. F. Jiang and C. H. Lai, J. Magn. Magn. Mater. **272-276**, 2312 (2004).
[14] P. F. Carcia, J. Appl. Phys. **63**, 5066 (1988).
[15] B. N. Engel, C. D. England, R. A. Van Leeuwen, M. H. Wiedmann, and C. M. Falco, Phys. Rev. Lett. **67**, 1910 (1991).
[16] H. Fuke, K. Saito, Y. Kamiguchi, H. Iwasaki, and M. Sahashi, J. Appl. Phys. **81**, 4004 (1997).
[17] A. J. Devasahayam, P. J. Sides, and M. Kryder, J. Appl. Phys. **83**, 7216 (1998).
[18] J. Ferré, *Spin Dynamics in Confined Magnetic Structures I* (Springer-Verlag, Berlin, 2002), p. 127.
[19] F. Romanens, S. Pizzini, F. Yokaichiya, M. Bonfim, Y. Pennec, J. Camarero, J. Vogel, J. Sort, F. Garcia, B. Rodmacq, and B. Dieny, Phys. Rev. B **72**, 134410 (2005).
[20] F. Romanens, S. Pizzini, J. Sort, F. Garcia, J. Camarero, F. Yokaichiya, Y. Pennec, J. Vogel, and B. Dieny, Eur. Phys. J. B **45**, 185 (2005).
[21] N. Nakajima, T. Koide, T. Shidara, H. Miyauchi, H. Fukutani, A. Fujimori, K. Iio, T. Katayama, M. Nyvlt, and Y. Suzuki, Phys. Rev. Lett. **81**, 5229 (1998).
[22] D. Blavette, B. Deconihout, A. Bostel, J.-M. Sarrau, M. Bouet, and A. Menand, Rev. Sci. Instrum. **64**, 2911 (1993).
[23] D. Blavette, B. Deconihout, S. Chambreland, and A. Bostel, Ultramicroscopy **70**, 115 (1998).
[24] X. W. Zhou, H. N. G. Wadley, R. A. Johnson, D. J. Larson, N. Tabat, A. Cerezo, A. K. Petford-Long, G. D. W. Smith, P. H. Clifton, R. L. Martens, and T. F. Kelly, Acta Mater. **49**, 4005 (2001).
[25] D. J. Larson, A. K. Petford-Long, Y. Q. Ma, and A. Cerezo, Acta Mater. **52**, 2847 (2004).
[26] D. J. Larson, Thin Solid Films **505**, 16 (2006).
[27] A. Grenier, R. Lardé, E. Cadel, F. Vurpillot, J. Juraszek, J. Teillet, and N. Tiercelin, J. Appl. Phys. **102**, 033912 (2007).
[28] A. Zarefy, R. Lardé, L. Lechevallier, F. Cuvilly, J.-M. Le Breton, B. Rodmacq, and B. Dieny, J. Magn. Magn. Mater. (to be published).
[29] A. Zarefy, R. Lardé, L. Lechevallier, F. Cuvilly, J.-M. Le Breton, B. Rodmacq, and B. Dieny, J. Appl. Phys. (to be published).
[30] R. Lardé, L. Lechevallier, A. Zarefy, A. Bostel, J. Juraszek, J.-M. Le Breton, B. Rodmacq, and B. Dieny, J. Appl. Phys. **105**, 084307 (2009).
[31] A. A. Ayon, R. Braff, C. C. Lin, H. H. Swain, and M. A. Schmidt, J. Electrochem. Soc. **146**, 339 (1999).
[32] B. Gault, F. Vurpillot, A. Vella, M. Gilbert, A. Menand, D. Blavette, and B. Deconihout, Rev. Sci. Instrum. **77**, 043705 (2006).
[33] P. Bas, A. Bostel, B. Deconihout, and D. Blavette, Appl. Surf. Sci. **87-88**, 298 (1995).
[34] SIMULREFLECT at www.drecam.cea.fr/llb/prism/programs.html
[35] X. Ji, H. Ju, D. E. Mc Cready, and K. M. Krishnan, J. Appl. Phys. **98**, 116101 (2005).
[36] Z. G. Li and P. F. Carcia, J. Appl. Phys. **71**, 842 (1992).
[37] J. Kanak, T. Stobiecki, and S. Van Dijken, IEEE Trans. Magn. **44**, 238 (2008).
[38] J. C. S. Kools, J. Appl. Phys. **77**, 2993 (1995).
[39] X. W. Zhou and H. N. G. Wadley, J. Appl. Phys. **84**, 2301 (1998).
[40] J. Sort, B. Dieny, and J. Noguès, Phys. Rev. B **72**, 104412 (2005).
[41] C. Kittel, Phys. Rev. **70**, 965 (1946).
[42] S. Hashimoto, Y. Ochiai, and K. Aso, J. Appl. Phys. **67**, 4429 (1990).
[43] V. Gehanno, Y. Samson, A. Marty, B. Gilles, and A. Chamberod, J. Magn. Magn. Mater. **172**, 26 (1997).
[44] J. Camarero, Y. Pennec, J. Vogel, M. Bonfim, S. Pizzini, F. Ernult, F. Fettar, F. Garcia, F. Lançon, L. Billard, B. Dieny, A. Tagliaferri, and N. B. Brookes Phys. Rev. Lett. **91**, 027201 (2003).
[45] V. Baltz, A. Marty, B. Rodmacq, and B. Dieny, Phys. Rev. B **75**, 014406 (2007).